

This is an Open Access document downloaded from ORCA, Cardiff University's institutional repository:<https://orca.cardiff.ac.uk/id/eprint/153719/>

This is the author's version of a work that was submitted to / accepted for publication.

Citation for final published version:

Liang, Yu, Douthwaite, Mark, Huang, Xiaoyang, Zhao, Binbin, Tang, Qiong, Liu, Lei and Dong, Jinxiang 2023. Zero-oxidation state precursor assisted fabrication of highly dispersed and stable Pt catalyst for chemoselective hydrogenation of  $\alpha,\beta$ -unsaturated aldehydes. *Nano Research* 16 , pp. 6085-6093.  
10.1007/s12274-022-4822-4

Publishers page: <http://dx.doi.org/10.1007/s12274-022-4822-4>

Please note:

Changes made as a result of publishing processes such as copy-editing, formatting and page numbers may not be reflected in this version. For the definitive version of this publication, please refer to the published source. You are advised to consult the publisher's version if you wish to cite this paper.

This version is being made available in accordance with publisher policies. See <http://orca.cf.ac.uk/policies.html> for usage policies. Copyright and moral rights for publications made available in ORCA are retained by the copyright holders.



# Zero-oxidation state precursor assisted fabrication of highly dispersed and stable Pt catalyst for chemoselective hydrogenation of $\alpha$ , $\beta$ -unsaturated aldehydes

Yu Liang<sup>a</sup>, Mark Douthwaite<sup>b</sup>, Xiaoyang Huang<sup>b</sup>, Binbin Zhao<sup>a</sup>, Qiong Tang<sup>a</sup>, Lei Liu<sup>a,\*</sup>, and Jinxiang Dong<sup>a</sup>

<sup>a</sup>College of Chemical Engineering and Technology, Taiyuan University of Technology, Yingze West Street 79, Taiyuan 030024, Shanxi, China.

<sup>b</sup>Cardiff Catalysis Institute, School of Chemistry, Cardiff University, Main Building, Park Place, Cardiff, CF10 3AT, United Kingdom

\*Corresponding Authors: Prof. Lei Liu, liulei@tyut.edu.cn

**ABSTRACT:** The chemoselective hydrogenation of  $\alpha$ ,  $\beta$ -unsaturated aldehydes is a key strategy for the synthesis of fine chemicals. Herein, we developed an efficient method of depositing Pt particles on FeO<sub>x</sub>/SBA-15. This strategy is dependent on using a platinum-divinyltetramethyldisiloxane complex (Pt<sup>0</sup>-DVTMS) as the precursor, which we demonstrate can be removed through a H<sub>2</sub>-treatment under mild conditions. This, in turn, allowed for the synthesis of catalysts with well dispersed Pt particles. The presence of FeO<sub>x</sub> species also aided Pt dispersion; when coated onto SBA-15, FeO<sub>x</sub> strongly interacted with dissociated Pt species, inhibiting both Pt aggregation and metal leaching. Using cinnamaldehyde as a model  $\alpha$ ,  $\beta$ -unsaturated aldehyde, it was demonstrated that this catalyst was highly selective towards the unsaturated alcohol and no obvious loss in activity was observed over five recycles. This catalyst was determined to be significantly more effective than an analogous catalyst prepared using chloroplatinic acid as a precursor, evidencing the importance of using the Pt<sup>0</sup>-DVTMS precursor. We corroborate the excellent catalytic performance to highly dispersed Pt-species, whereby Pt<sup>0</sup> and Pt<sup>2+</sup> play a critical role in activating H<sub>2</sub> and the C=O bond. This research demonstrates that the Pt precursor can have a significant impact on the physicochemical properties and thus, the performance of the final catalyst. It also evidences how metal support interactions can dramatically influence selectivity in such

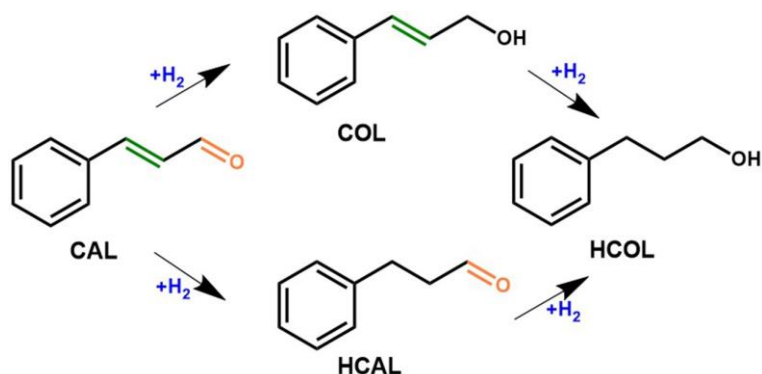
hydrogenation reactions. This novel catalyst preparation protocol, using a DVTMS ligand for Pt impregnation, offers a facile approach to the design of multi-component heterogeneous catalysts.

**Key Words:** platinum catalyst, zero-oxidation state, stability, chemoselective hydrogenation,  $\alpha$ ,  $\beta$ -unsaturated aldehydes

## 1. Introduction

Selective hydrogenation of  $\alpha$ ,  $\beta$ -unsaturated aldehydes to produce fine chemicals is an important industrial process which has been investigated extensively [1-3]. Despite the progress made in this field, designing heterogeneous catalysts which are chemoselective remains a grand challenge [4]. This is especially true for the selective hydrogenation of C=O bonds (715 kJ/mol) as they possess a higher bond energy than the adjacent C=C moiety (615 kJ/mol). The  $\eta_4$  adsorption mode also thermodynamically favours C=C bond hydrogenation, making the selective hydrogenation of carbonyl species even more challenging [5]. Cinnamaldehyde (CAL) is a typical model compound used to study the chemoselective hydrogenation of  $\alpha$ ,  $\beta$ -unsaturated aldehydes. CAL (Scheme 1) can undergo hydrogenation at either (or both) of its C=C or C=O groups, leading to the formation of hydrocinnamaldehyde (HCAL), cinnamyl alcohol (COL), and hydrocinnamyl alcohol (HCOL) [6]. Supported precious metal catalysts (*i.e.* Pt, Au, and Ir) are often used for this reaction, however, some auxiliaries or modifiers such as Sn, Fe, Co, Ni, *etc.* [7-9] are generally required to enhance the selectivity towards the unsaturated alcohol. Interestingly, Pt has been determined to form intermetallic nanoparticles with the promoters mentioned above, tuning the electronic structure of primary active metals to facilitate selective hydrogenation [10-14]. Reducible metal oxides (FeO<sub>x</sub>, MoO<sub>x</sub>, CeO<sub>x</sub>, NbO<sub>x</sub>, *etc.*) are often used to cooperate with precious metals in these systems. The presence of electrophilic sites on these metal oxides can preferentially adsorb and activate the C=O bonds, before a consecutive reaction with activated H-species over the adjacent noble metals occurs to form unsaturated alcohols [15-18]. Such catalytic performance could

be improved by enhancing the synergetic effect of Pt and metal oxides, which is associated with the distribution and intimate interaction of Pt and the electrophilic sites. However, to date, examples of active noble metals (in previous studies) usually existed on the surface of the support. Moreover, the low efficiency of noble metals is not conducive to industrial applications.



**Scheme 1** Reaction routes for the hydrogenation of cinnamaldehyde: CAL for cinnamaldehyde, COL for cinnamyl alcohol, HCAL for hydrocinnamaldehyde, HCOL for hydrocinnamyl alcohol.

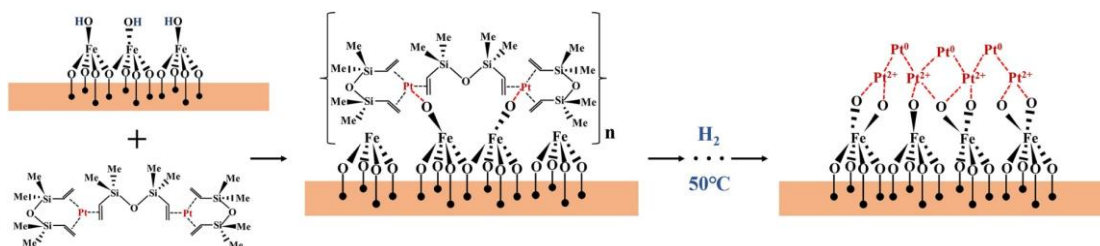
Recently, the selective hydrogenation of 4-nitrostyrene towards 4-aminostyrene was achieved (*i.e.* Pt/FeO<sub>x</sub> catalyst with TOF of 1500 h<sup>-1</sup> and selectivity of 99%) over highly dispersed or single-site Pt catalysts, wherein supported atomic Pt species were found to inhibit the hydrogenation of the C=C moiety [19,20]. It is well known that isolated metal atoms, possessing high surface energies, tend to aggregate and form nanoparticles, especially under harsh preparation or reaction conditions [21]. Therefore, to fabricate a highly dispersed (and stable) Pt-based catalyst, a strong interaction between the metal and support is required [22-26].

Previously, the metal precursors (metal salts and organometallic complexes) used in the preparation of these materials have been reported to be important in controlling the dispersion of the metal surface species [27-30]. In the case of organometallic complexes, organic ligands can effectively isolate and protect the metal centre. Thus, in principle, using an organometallic complex as a metal precursor could be an effective method for obtaining highly dispersed metal catalysts [31-35]. A limiting step,

however, is likely to be the removal of the organic species which are coordinated to the metal. This is critical for exposing the metal atoms on the support [36]. To do this, the conventional approach is usually to employ a thermal heat treatment [37]. However, harsh reductive conditions can promote metal aggregation, leading to the formation of nanoparticles [38]. Consequently, it is important that a method for the removal of these ligands, under mild conditions, is developed, to suppress undesirable aggregation of the remaining metal species on the support. For example, atomically dispersed Pd on graphene was previously prepared using palladium hexafluoroacetylacetonate as a metal precursor, which was treated under O<sub>3</sub> to promote ligand degradation [39]. Gates *et al.* [37] also successfully obtained Au single sites supported on a NaY zeolite using an Au(CH<sub>3</sub>)<sub>2</sub>(acac) as a precursor. The authors determined that the acac ligands could be rapidly detached through exposure of the material to CO and O<sub>2</sub>. This led to the isolation of Au species, confined within NaY zeolite channels.

Based on this previous research, we opted to use a platinum-divinyltetramethyldisiloxane complex [Pt<sup>0</sup>-DVTMS] precursor for the preparation of Pt supported on FeO<sub>x</sub>/SBA-15 (and associated composites). Such precursor was widely applied in the hydrosilylation reaction [40], in which Pt-species existed in the form of zero-oxidation state, and the coordination of Pt and C=C bond of the ligand was easy to destroy during the reaction. Herein, we demonstrate that a primary benefit of this precursor is that, when deposited onto the support, it can be removed under a flow of H<sub>2</sub> at relatively mild conditions. This, in turn, allows for the preparation of highly dispersed Pt catalysts. An illustrative example of how this is proposed to proceed on an FeO<sub>x</sub>/SBA-15 support is presented in Scheme 2; Metallic Pt atoms promote the activation of H<sub>2</sub>, which subsequently hydrogenates the C=C bond in the ligand. As a result, it breaks the coordination between the Pt and ligand, leading to the decomposition of the complex on the support surface and the formation of finely distributed Pt species. Furthermore, we demonstrate that the reducible FeO<sub>x</sub> phase, coated onto the SBA-15, is highly effective at anchoring the Pt species; aggregation of Pt was suppressed under reaction conditions. The Pt/FeO<sub>x</sub>/SBA-15 catalyst exhibited

excellent catalytic performance for the selective hydrogenation of CAL to COL, and the universality of this chemoselectivity was evidenced through use of other unsaturated aldehydes, *i.e.* trans-4-methylcinnamaldehyde, 3-(2-furyl) acrolein, and 3-methyl-2-butenal. Our work offers a new approach for the design of well dispersed, multi-component chemoselective heterogeneous catalysts.



**Scheme 2** Procedure for locating of Pt<sup>0</sup>-DVTMS on FeO<sub>x</sub>/SBA-15, followed by hydrogenolysis to form Pt/FeO<sub>x</sub>/SBA-15 catalysts

## 2. Experimental section

### 2.1 Synthesis of the support FeO<sub>x</sub>/SBA-15

The 10 wt.%FeO<sub>x</sub>/SBA-15 supports were prepared via an impregnation method using an aqueous solution of Fe(NO<sub>3</sub>)<sub>3</sub>·9H<sub>2</sub>O. The impregnated sample was firstly calcined at 400 °C in air for 5 h, then thermal treated at 800 °C in Ar for 3 h.

### 2.2 Synthesis of the catalyst Pt/FeO<sub>x</sub>/SBA-15

FeO<sub>x</sub>/SBA-15 supported Pt catalysts were prepared through incipient wetness impregnation using Platinum-divinyltetramethyldisiloxane complex as a precursor in xylene solvent. The products were reduced at 50 °C in H<sub>2</sub> for 3 h, designed as Pt/FeO<sub>x</sub>/SBA-15. The resulting Pt and Fe loading (in weight percentage metal) of some of the samples was checked by ICP and was found to be within the error of measurement of the after preparation expected loading.

The details of the synthesis, characterization techniques, and catalytic selective hydrogenation are given in the supplementary data.

## 3. Results and discussion

### 3.1 Catalyst characterization

First, SBA-15 was impregnated with  $\text{Fe}(\text{NO}_3)_3 \cdot 9\text{H}_2\text{O}$  and thermally treated to produce a 10 wt.%  $\text{FeO}_x/\text{SBA-15}$  material. Subsequent characterisation of this material by powder X-ray diffraction (XRD) (Figure 1 and S1) confirmed that the material had retained its mesoporous structure [41]. The reflections observed from XRD of the  $\text{FeO}_x/\text{SBA-15}$  sample were indexed to a pure rhombohedral phase of  $\alpha\text{-Fe}_2\text{O}_3$  [space group: R-3c (167)] [42]. Probing this material by UV-vis spectroscopy (Figure S2) provided further evidence for this; a characteristic absorption at 554 nm was observed [42]. Similar conclusions could be drawn from analysis of the sample by X-ray photoelectron spectroscopy (XPS). The binding energy of peaks (*ca.* 711 eV) observed in the Fe 2p region for  $\text{FeO}_x/\text{SBA-15}$  and  $\text{Pt}/\text{FeO}_x/\text{SBA-15}$  materials (Figure S3) are characteristic of Fe 2p<sub>3/2</sub> in  $\text{Fe}^{3+}$  ions within an  $\alpha\text{-Fe}_2\text{O}_3$  phase [43]. Therefore, based on the XRD, UV-vis and XPS results, it can be stated that the Fe oxide component consisted of  $\alpha\text{-Fe}_2\text{O}_3$ , which remained unchanged after their impregnation with  $\text{Pt}^0\text{-DVTMS}$  and after its thermal reduction at 50 °C (Figure 1, S2 and S3). To further assess whether changes to the structural and textural properties had occurred through Pt incorporation into the materials, the series of materials were probed by  $\text{N}_2$  physisorption. The corresponding adsorption–desorption isotherms are illustrated in Figure S4. Through analysis of the desorption curves using the BJH method [44], it was clear that no notable changes to the average pore diameters had occurred through incorporation of  $\text{FeO}_x$  and Pt; all were in the range of 10.2-10.8 nm (Table 1). By contrast, the BET specific surface area and the pore volume of the catalysts decreased compared to the bare SBA-15 support, indicating that the  $\text{FeO}_x$  and Pt were situated within its mesoporous channels [13,45]. The absence of Pt diffraction peaks (Figure 1) however, confirmed that the Pt species were highly dispersed on the support after loading.

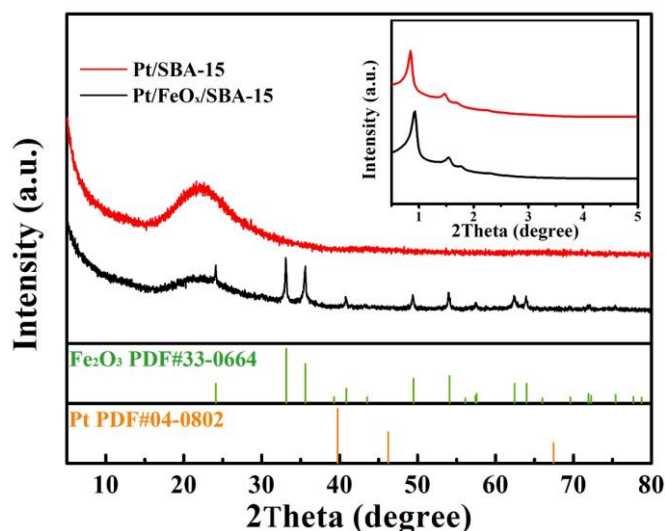


**Figure 1** Powder XRD patterns of the supported Pt catalysts on Fe<sub>2</sub>O<sub>3</sub>-modified SBA-15 as well as the pristine SBA-15.

As discussed in the introduction, Pt<sup>0</sup>-DVTMS was used as the Pt precursor as it was hypothesized that the DVTMS ligands could be removed under mild reductive conditions. To investigate this, *in-situ* diffuse reflectance infrared Fourier transform spectroscopy (DRIFTS) was employed, under a flow of H<sub>2</sub>. For these experiments, the platinum-complex and FeO<sub>x</sub>/SBA-15 supports were exposed to a hydrogen stream for 3 hours to remove ligand (10 vol.%H<sub>2</sub>/Ar, 50 mL/min, 50 °C). The introduction of H<sub>2</sub> resulted in the gradual disappearance of characteristic bands of C=C moieties at 3000-3100 cm<sup>-1</sup> (Figure 2a), it is attributed to the saturation of double bonds in the ligand [45]. It is well established that Pt<sup>0</sup> is highly beneficial for the activation of H<sub>2</sub> [46,47]. And as such, it's hypothesized that these species are involved in the reduction of these moieties. Further insight on the state of Pt in these species was acquired by assessing peaks indicative of Pt-ligand bonding at *ca.* 834, and 750-770 cm<sup>-1</sup>. Upon H<sub>2</sub> exposure, these peaks disappeared confirming the cleavage of platinum-complex bonds [48]. To confirm that the ligand had successfully been removed from the sample, the post reduction sample was subjected to TG-MS under a flow of air (180 mL/min). Only a 0.2% mass loss was observed and there was no evidence to suggest that any CO or CO<sub>2</sub> was emitted. This confirmed that the reduction process had been successful, and no ligand remained on the surface of the sample. Given that the C=C bonds disappeared simultaneously with the disappearance of ligand and ligand-Pt stretches, we

hypothesize that Pt likely anchors to the support through hydrogenolysis [40]. Ultimately, this confirmed that our hypothesis was correct; only a gentle reduction treatment was required for the preparation of the final catalyst.

**Table 1** Physicochemical parameters of the synthetic catalysts

Samples	S <sub>BET</sub> (m <sup>2</sup> /g)	V <sub>P</sub> (cm <sup>3</sup> /g)	Pore diameter (Å)	Pt/Fe loading (wt.%)
SBA-15	474.13	1.17	106	
FeO <sub>x</sub> /SBA-15	406.54	0.97	102	10.22 (Fe)
Pt/FeO <sub>x</sub> /SBA-15	380.27	0.91	103	0.377
Pt/SBA-15	461.09	1.16	108	0.389
Pt/FeO <sub>x</sub> /SBA-15-C	389.40	0.90	101	0.490

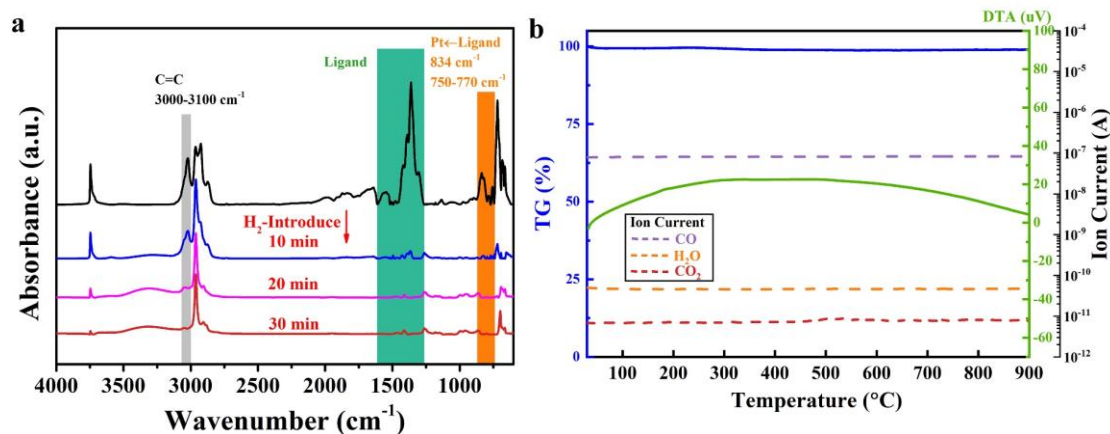


**Figure 2** The characteristic results for the removal of organic ligands: (a) *In-situ* FTIR spectra of Pt<sup>0</sup>-DVTMS loading at FeO<sub>x</sub>/SBA-15 under H<sub>2</sub> flow at synthetic condition; (b) TG-MS profile of FeO<sub>x</sub>/SBA-15 containing Pt<sup>0</sup>-DVTMS after H<sub>2</sub>-treatment under air.

High-resolution transmission electron microscopy (HRTEM) micrographs of the SBA-15 confirmed existence of hexagonal pores that were highly uniform and ordered, which is characteristic of this material [21]. After coating FeO<sub>x</sub> onto the SBA-15, many FeO<sub>x</sub> nanoparticles (~6 nm) were evidently distributed within these channels (Figure S5a). Figure 3 presents the bright-field HRTEM micrographs with particle size distributions of the catalysts which were prepared. For the Pt/FeO<sub>x</sub>/SBA-15 material, 0.368 and 0.27 nm lattices spacing were observed, originating from the Fe<sub>2</sub>O<sub>3</sub> (012) and (104), respectively. Interestingly, no Pt species could be observed on the materials surface, providing further evidence that the Pt component was highly dispersed on the

FeO<sub>x</sub>/SBA-15 support (Figure 3a and b). Figure 1 presents XRD results that are consistent with this conclusion. On the contrary, for the Pt/SBA-15 material, Pt particles were clearly visible; the size of Pt particles was close to ~3 nm on average (Figure 3c). TEM micrographs of the Pt/SBA-15 material showed that Pt particles were actually shed from the support. This is attributed to the method of preparing the samples for analysis, where samples are first dispersed in ethanol and sonicated, prior to spraying on a copper microgrid. What this suggests is that the Pt particles in the Pt/SBA-15 material must interact weakly with the support. Given that this phenomenon was not observed with Pt/FeO<sub>x</sub>/SBA-15 material, suggesting that the presence of FeO<sub>x</sub> could increase interactions between Pt and support.

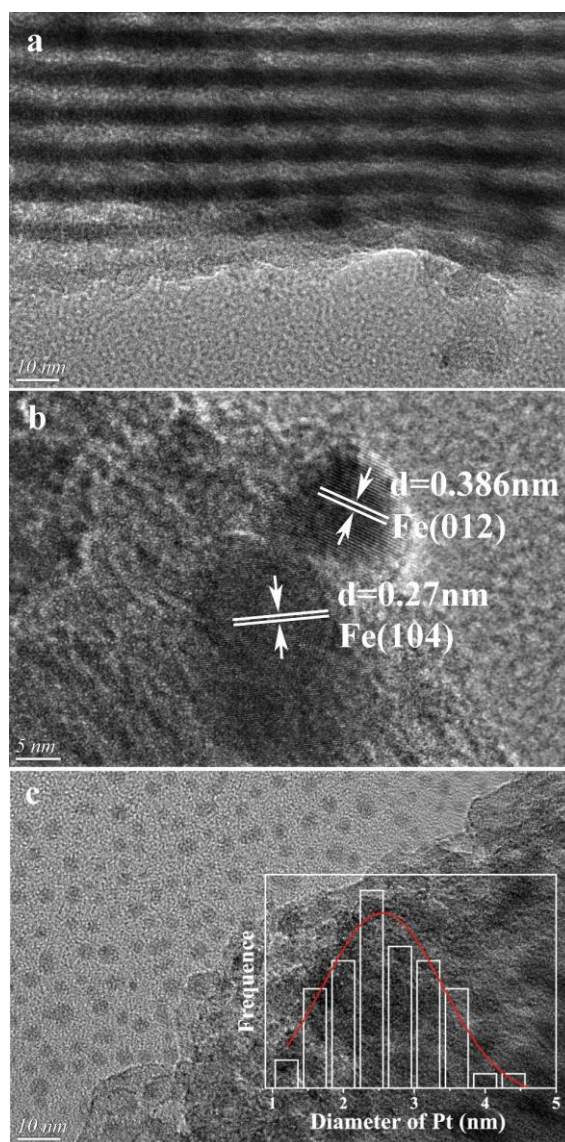


**Figure 3** HRTEM images and particle size distributions of (a, b) Pt/FeO<sub>x</sub>/SBA-15 and (c) Pt/SBA-15 catalysts.

To further probe the microstructure of the Pt/FeO<sub>x</sub>/SBA-15 material, high angle angular dark field-scanning transmission electron microscopy (HAADF-STEM) was employed. Energy dispersive X-ray spectroscopy (EDS) measurements, illustrated in Figure 4, confirmed the presence of Pt, Fe and Si in the sample [13]. In conclusion, the majority of Pt species present are coated onto the FeO<sub>x</sub> component from this experiment. From the associated HAADF-STEM micrographs (representative example presented in Figure 5, an average particle size of ~1.3 nm was determined. The mean Pt particle size present in the Pt/FeO<sub>x</sub>/SBA-15 material was evidently far smaller than that present in both analogous materials; the Pt/SBA-15 material (Figure 3b, Pt particles was close to ~3 nm) and the Pt/FeO<sub>x</sub>/SBA-15-C material (Figure S5c, Pt/FeO<sub>x</sub>/SBA-15-C were prepared using an impregnation method with H<sub>2</sub>PtCl<sub>6</sub> and Pt particles was close to ~4.3 nm). In summary, the microscopy experiments provide direct evidence that the presence of FeO<sub>x</sub> and choice of Pt precursor dramatically influences Pt dispersion.

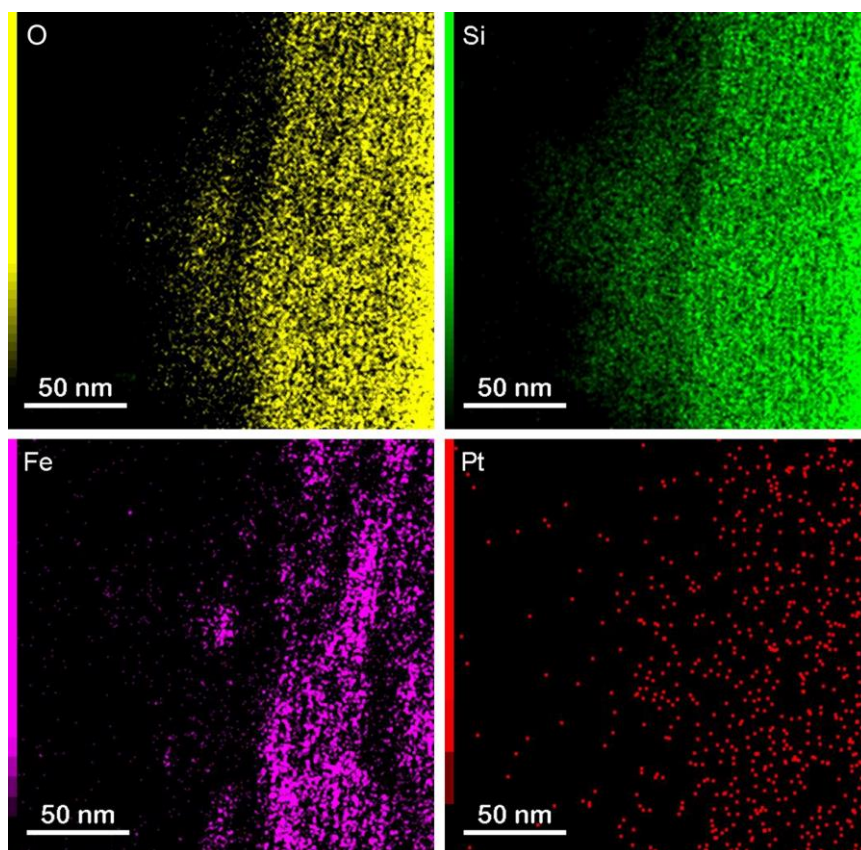


**Figure 4** HAADF-STEM elemental mapping images of Pt/FeO<sub>x</sub>/SBA-15 catalyst.

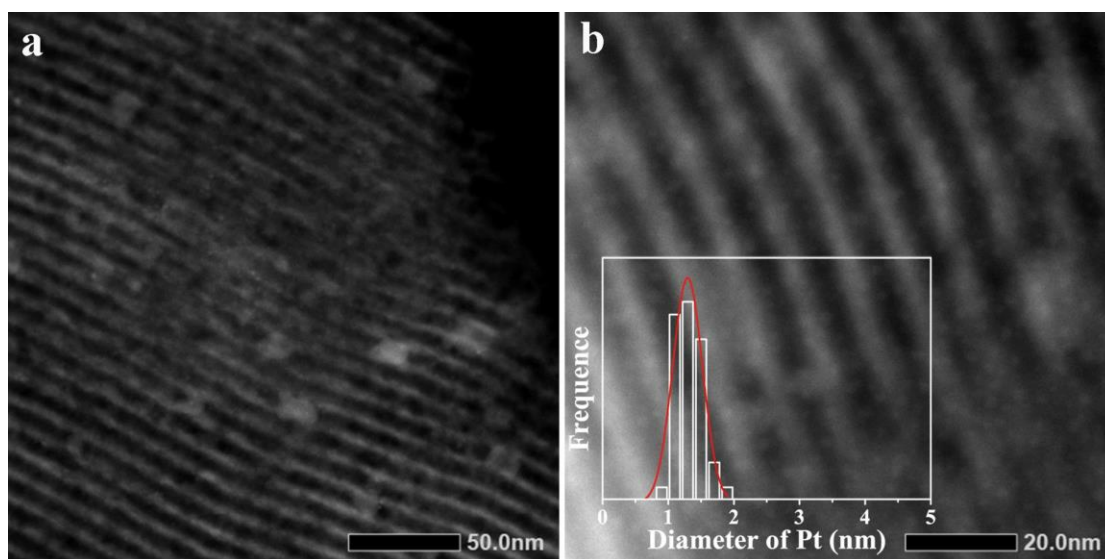


**Figure 5** HAADF-STEM images and particle size distributions of Pt/FeO<sub>x</sub>/SBA-15 catalyst.

Following on from this, *in-situ* DRIFTS spectras with CO were performed to acquire further evidence of Pt dispersion in the material (Figure 6) [49,50]. A strong vibrational band at *ca.* 2075 cm<sup>-1</sup> was observed over all the materials, whereas a series of weaker bands, at *ca.* 1850 cm<sup>-1</sup>, was only observed in the spectra of the Pt/SBA-15 and Pt/FeO<sub>x</sub>/SBA-15-C materials. Over Pt supported catalysts, bands at *ca.* 1850 cm<sup>-1</sup> are typically attributed to bridged adsorption of CO on Pt nanoparticles [27,51]. Notably, the exact energy of the linear CO stretch (strong adsorption band at *ca.* 2075 cm<sup>-1</sup>) over different samples was slightly different. A blue shift was observed for the linear adsorption band in the Pt/FeO<sub>x</sub>/SBA-15 material. Blue shifts of this nature are typically associated with changes in the electronic properties of the FeO<sub>x</sub> particle, which can be induced either through differing metal-support interactions or a change in particle size [52]. Collectively, these experiments provide further evidence that Pt dispersion is greater in the Pt/FeO<sub>x</sub>/SBA-15 material which was prepared using the Pt<sup>0</sup>-DVTMS precursor, which is in agreement with the prior microscopy data presented.

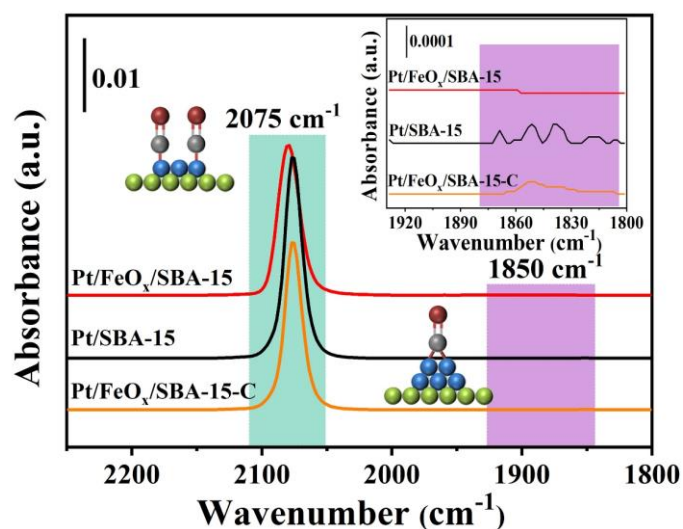
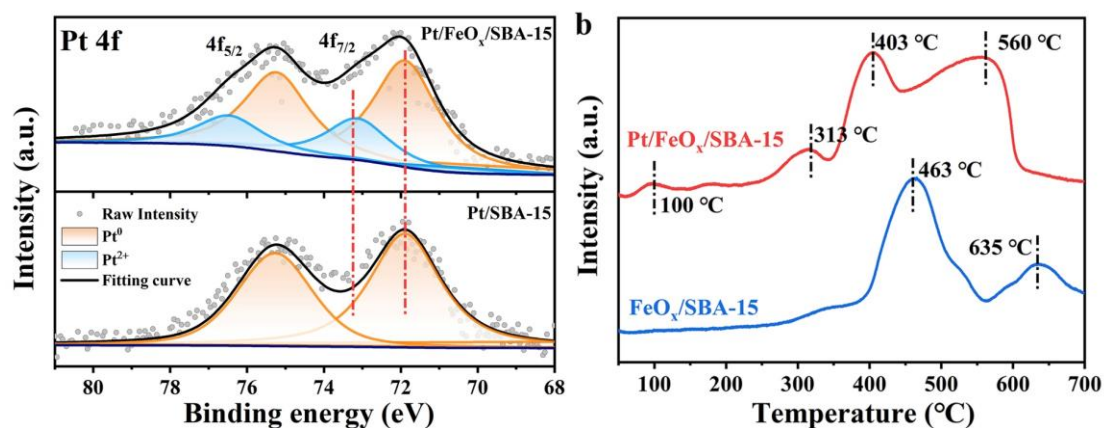


Figure 6 *In-situ* CO-DRIFT spectra of various Pt-based catalysts.

The chemical state of the Pt species in each of the materials was subsequently identified by XPS. Figure 7a confirms that Pt<sup>0</sup> and Pt<sup>2+</sup> species co-exist in Pt/FeO<sub>x</sub>/SBA-15 material, which correspond to the binding energies observed at 71.88 eV and 73.12 eV [6], respectively. Over the Pt/SBA-15 material, only the peak at a binding energy of 71.86 eV was observed, confirming that only Pt<sup>0</sup> species were present in this sample. In the Pt/FeO<sub>x</sub>/SBA-15 material Pt<sup>2+</sup> accounted for *ca.* 27.7% of the total peak area of Pt<sup>2+</sup> and Pt<sup>0</sup>. The increased proportion of Pt<sup>2+</sup> in this material is likely to be indicate of PtO and could again provide insight on how the presence of the FeO<sub>x</sub> sub-layer might influence the electronic properties of the Pt species. The donation of electron density into the FeO<sub>x</sub> from the Pt nanoparticle could, in theory, make the Pt more prone to oxidation through exposure to air after the thermal reduction process. If this hypothesis is correct, it could also provide an explanation as to why there is a greater interaction between Pt and the FeO<sub>x</sub>/SBA-15 support. This, in turn, could explain why a higher Pt dispersion is observed in this material [9], as opposed to the analogous Pt/SBA-15 catalyst, which leached during the preparation of samples for TEM.

Temperature-programmed reduction with hydrogen (H<sub>2</sub>-TPR) profiles (Figure 7b) were subsequently conducted to gain further insight on the interactions between the Pt and FeO<sub>x</sub> components in the Pt/FeO<sub>x</sub>/SBA-15 material. Peaks at around 100 °C were

ascribed to the reduction of the positively charged  $\text{Pt}^{2+}$  species [53]. The TPR profiles for Pt/FeO<sub>x</sub>/SBA-15 catalyst feature a prominent peak at around 350-700 °C which was generally attributed to the reduction of Fe<sub>2</sub>O<sub>3</sub> species. More details, the peak at around 463 °C is due to the reduction of Fe<sub>2</sub>O<sub>3</sub> to Fe<sub>3</sub>O<sub>4</sub>, and a broad peak at around 635 °C can be corresponding to the reduction of Fe<sub>3</sub>O<sub>4</sub> to FeO and metallic Fe. As the reduction of FeO<sub>x</sub> oxides was enhanced by the hydrogen spillover effect of Pt, the reduction peak of Fe oxides shifts from 463 °C to 403 °C with Pt loading onto FeO<sub>x</sub>/SBA-15 supports, strong interactions between Pt and FeO<sub>x</sub> are evident. Besides, the new peak at 313 °C can be attributed to the synergistic effect between the Fe<sub>2</sub>O<sub>3</sub> and  $\text{Pt}^{2+}$  active species, which can greatly facilitate the redox potential of the catalyst. On recalling the TEM and H<sub>2</sub>-TPR results, the selective deposition of Pt on Fe *via* mild reduction of  $\text{Pt}^0$ -DVTMS complex precursors would lead to the direct formation of finely distributed  $\text{Pt}^{2+}$  species on the FeO<sub>x</sub> metal surface, which generates a strong contact between Pt and FeO<sub>x</sub> and promotes the reduction of FeO<sub>x</sub> during the TPR detection [29].



**Figure 7** The characterization results of Pt-FeO<sub>x</sub> interaction: (a) Pt 4f XPS spectra of Pt on FeO<sub>x</sub>-containing SBA-15 as well as pristine SBA-15; (b) H<sub>2</sub>-TPR profiles of FeO<sub>x</sub>/SBA-15 before and after loading Pt.

### 3.2 Catalytic performance

The series of materials were subsequently employed as catalysts for CAL hydrogenation. The performance exhibited by each of the materials is presented in Figure 8 Table S1. Of the catalysts, Pt/FeO<sub>x</sub>/SBA-15 exhibited the highest catalytic

performance. Perhaps more interestingly, this catalyst was determined to be significantly more selective to COL than the other catalysts. This catalyst evidently promoted C=O reduction over C=C; the thermodynamically more challenging moiety to hydrogenate. When the performance of this catalyst was compared with the analogous Pt/SBA-15 and Pt/FeO<sub>x</sub>/SBA-15-C catalysts, where the latter was prepared using H<sub>2</sub>PtCl<sub>6</sub> as the precursor, some interesting conclusions can be made. The activity of the catalysts appeared to correlated well with Pt dispersion; CAL conversions of 88% and 28% were exhibited by the Pt/FeO<sub>x</sub>/SBA-15 and Pt/FeO<sub>x</sub>/SBA-15-C catalysts, respectively, which correlated with the mean Pt particle sizes they possessed (1.3 and 4.3 nm, respectively). These observations are further underlined through consulting the CO-DRIFTS experiments conducted (Figure 6).

More interesting conclusions can however be derived from the differences in chemoselectivity observed. A yield of COL of 72% was achieved over Pt/FeO<sub>x</sub>/SBA-15 catalyst, which is significantly about over 6 times higher than that of 14% for Pt/SBA-15, 12% for Pt/FeO<sub>x</sub>/SBA-15-C, and 5% for Pt<sup>0</sup>-DVTMS catalysts. When the hydrogenation was conducted in the presence of Pt<sup>0</sup>-DVTMS, homogeneously, a high activity was observed (85% conversion) but the selectivity to COL was extremely poor (5 %). Upon supporting (and reducing) this precursor onto SBA-15 (Pt-SBA-15), the activity dropped slightly (75% conversion) but selectivity to COL increased (18%). When impregnated and reduced onto the FeO<sub>x</sub>/SBA-15 however, the selectivity to COL increased dramatically (43%). Given that the observed selectivity to COL was significantly lower over the analogous Pt/FeO<sub>x</sub>/SBA-15 catalyst (82%), it is clear that both the Pt dispersion and active site environment strongly influence the chemoselectivity. When catalyst was used for hydrogenation, the Pt<sup>0</sup> species were beneficial to activation of the H<sub>2</sub>, and the Pt<sup>2+</sup> and Fe<sup>3+</sup> species (Figure 7 and S3) were beneficial for the preferential adsorption of the C=O group [54].

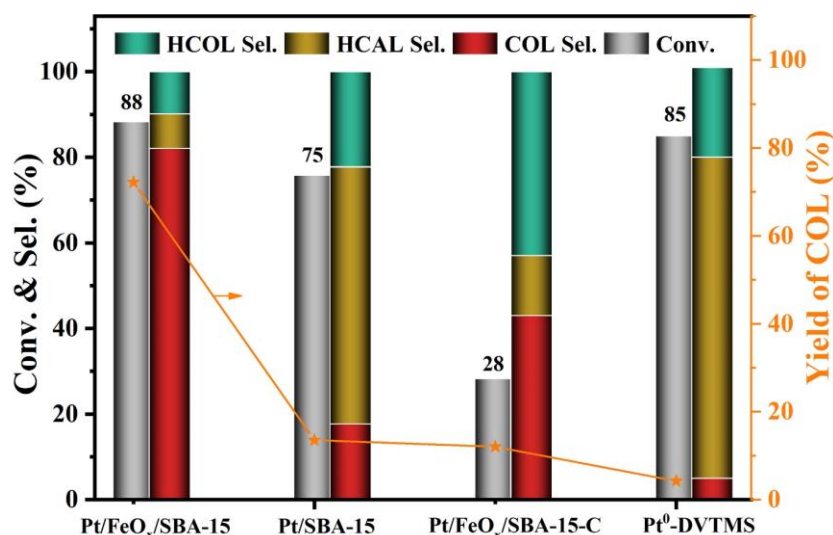


**Figure 8** Catalytic performances of CAL hydrogenation over various Pt-based catalyst.

(Reaction conditions: catalyst 20 mg, CAL 25 mmol, H<sub>2</sub> 3.0 MPa, ethanol 5 mL, time 30 min, temperature RT.)

The universality of the chemoselectivity exhibited by the Pt/FeO<sub>x</sub>/SBA-15 catalyst was subsequently probed. A series of other  $\alpha$ ,  $\beta$ -unsaturated aldehydes (A) were used as probe molecules (Table 2) [1]. With all substrates, the catalyst favored C=O hydrogenation over C=C obviously. That said, there is some evidence to suggest that the size of the R substituents influences the chemoselectivity. With a large, bulkier R-substituent, C=O hydrogenation becomes more favoured, suggesting that steric hinderance could influence the chemoselectivity. Thus, the mode of adsorption is clearly very important.

**Table 2** Catalytic performances of  $\alpha$ ,  $\beta$ -unsaturated aldehydes hydrogenation by Pt/FeO<sub>x</sub>/SBA-15 catalyst.

Reactant (A)	Conversion (%)	Selectivity (%)		
		B	C	D
	88.3	82.1	8.05	9.9
	100	85.6	0.8	13.5
	100	80.3	1.1	18.6
	64.9	72.1	3.3	24.6

**Reaction conditions:** catalyst 20 mg, reactant 25 mmol, H<sub>2</sub> 3.0 MPa, ethanol 5 mL, time 30 min, temperature RT.

The reusability of the Pt/FeO<sub>x</sub>/SBA-15 catalyst was subsequently assessed by performing repeat reactions using the same catalyst; five such cycles were conducted (Figure 9). No distinct loss in activity and or selectivity towards COL was observed even after five cycles. HAADF-STEM images (Figure S6) clearly show that the uniformity of the dispersed Pt clusters in the Pt/FeO<sub>x</sub>/SBA-15 catalyst was maintained; an average Pt particle size of ~1.3 nm was observed after five further cycles. Furthermore, XPS (Figure S7) confirmed that 24.5% of the Pt in the catalyst (after five cycles) consisted of Pt<sup>2+</sup>, which is only *ca.* 3% lower than in the fresh catalyst. This is further evidence that the structure of Pt/FeO<sub>x</sub>/SBA-15 catalyst remains unchanged after its use as a catalyst. To assess any Pt leached during the reaction, the post reaction solution was analyzed by ICP-OES. No Pt was detected, confirming that the strong interaction between Pt and FeO<sub>x</sub> is exhibited. The minor drop in CAL conversion over subsequent reactions, may simply be attributed to a minor decrease in the amount of catalyst present in the reactions; attributed to minor losses during the work-up and recycling process.

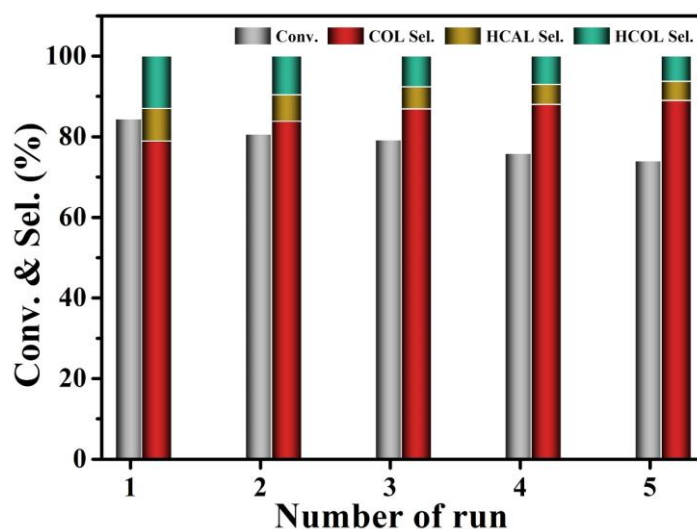


**Figure 9** Reusability of Pt/FeO<sub>x</sub>/SBA-15 catalyst for the CAL hydrogenation at 30 min.

Further investigations on the stability of Pt on the SBA-15 and FeO<sub>x</sub>/SBA-15 supports, in the reaction, were subsequently conducted. For this, a series hot filtration

experiments were run, whereby the catalyst was removed after 5-minutes of reaction and the reaction was run for a further 30 minutes (Table S2). With the Pt/FeO<sub>x</sub>/SBA-15 catalyst, no increase in CAL conversion was observed. On the contrary, with the Pt/SBA-15 catalyst, some further CAL conversion was observed. This further evidence that the presence of FeO<sub>x</sub> improves the interactions between Pt and support.

### 3.3 Proposed reaction mechanism

To probe the reaction mechanism over Pt/FeO<sub>x</sub>/SBA-15 catalyst, additional experiments were conducted using the reaction intermediates, COL and HCAL, as the substrates (Figure 10a). When COL was used as the reactant, a 7% conversion was observed. On the contrary, a 25% HCAL conversion was observed under the same reaction conditions. This trend was further emphasized when reactions were conducted over a (1:1) mixture of COL and HCAL; the conversion of COL dropped to 5.5 %, whereas the conversion of HCAL increased slightly to 26 %. Ultimately, these data clearly evidence that the C=O moiety is preferentially hydrogenated over Pt/FeO<sub>x</sub>/SBA-15 catalyst.

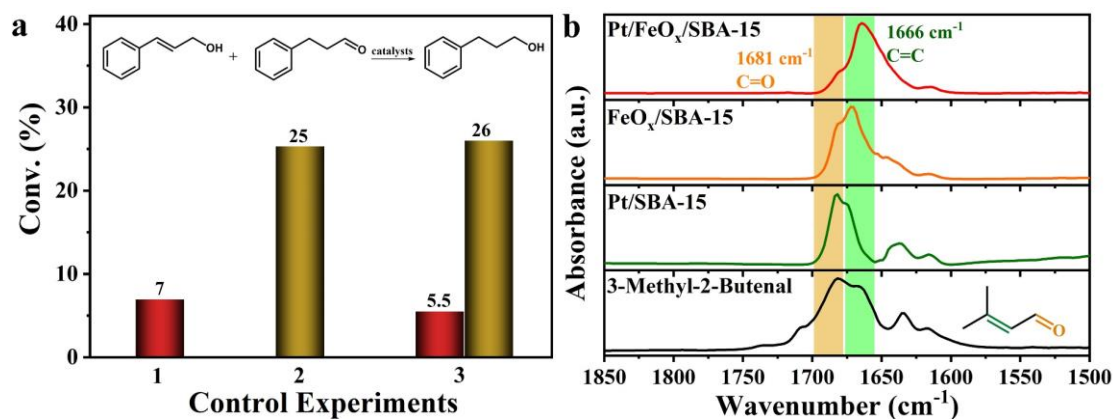


**Figure 10** (a) Conversion ratio of various substrates over Pt/FeO<sub>x</sub>/SBA-15 catalysts: substrate (25 mmol COL for Run1, 25 mmol HCAL for Run 2, 12.5 mmol COL and 12.5 mmol HCAL for Run 3), catalyst 20 mg, H<sub>2</sub> 3.0 MPa, ethanol 5 mL, 30 min. (b) *In-situ* DRIFTS of 3-methyl-2-butenal absorbed on various samples

To investigate the origin of this effect, *in-situ* DRIFTS experiments, using 3-methyl-2-butenal as a probe, were conducted over both the Pt/SBA-15 and Pt/FeO<sub>x</sub>/SBA-15 catalysts. The resultant spectra from these experiments are presented

in Figure 10b. Interestingly, the primary band associated with C=O vibration (*ca.* 1681  $\text{cm}^{-1}$ ) was slightly decrease in the experiment conducted over  $\text{FeO}_x/\text{SBA-15}$  and almost absent over  $\text{Pt}/\text{FeO}_x/\text{SBA-15}$  catalyst. The opposite was observed over  $\text{Pt}/\text{SBA-15}$  catalyst; adsorption bands indicative of C=C vibrations (at *ca.* 1666  $\text{cm}^{-1}$ ) were almost absent from spectrum taken over  $\text{Pt}/\text{SBA-15}$  catalyst, but clearly present over the analogous  $\text{Pt}/\text{FeO}_x/\text{SBA-15}$  catalyst. These experiments suggest that over  $\text{Pt}/\text{SBA-15}$  catalyst, the substrate preferentially adsorbs onto Pt sites *via* a  $\eta_4$  adsorption mode on the Pt active sites [5]. Whereas, over the decreased band associated with C=O vibration, over  $\text{Pt}/\text{FeO}_x/\text{SBA-15}$  catalyst, suggests that the  $\alpha$ ,  $\beta$ -unsaturated aldehyde predominantly adsorbs *via* the C=O bond [55]. These results evidence how the  $\text{FeO}_x$  dramatically influences the adsorption mode of the substrate, providing insight on why the chemoselectivity differs over the two catalysts.

Through combining the understanding derived from both the characterisation and catalytic testing, a reaction scheme for CAL hydrogenation over the  $\text{Pt}/\text{FeO}_x/\text{SBA-15}$  catalyst is proposed (Figure 11). Previous studies of Pt-based catalysts supported on metal-oxide have confirmed that Pt nanoparticles are active for C=C group hydrogenation. Research has indicated that the C=C groups hydrogenation is highly sensitive to particle size, with the rate of C=C hydrogenation increasing with metal particle size increasing [56]. Enhancements in C=O hydrogenation selectivity can however be promoted through the modification of interface sites between Pt and a surface metal oxide [24]. Pt- $\text{FeO}_x$  composites, in particular, which involve an ensemble of  $\text{Pt}^{2+}$  ions and Fe atoms or oxygen vacancies at the Pt- $\text{FeO}_x$  interface, have been demonstrated to be highly effective for several selective hydrogenation/oxidation reactions [22,25]. From the work presented herein, this is evidently also true for the  $\alpha$ ,  $\beta$ -unsaturated aldehydes hydrogenation. The presence of  $\text{FeO}_x$  clearly improves the dispersion and stability of surface Pt species but also, influences the adsorption mode and activation pathway of the substrate.

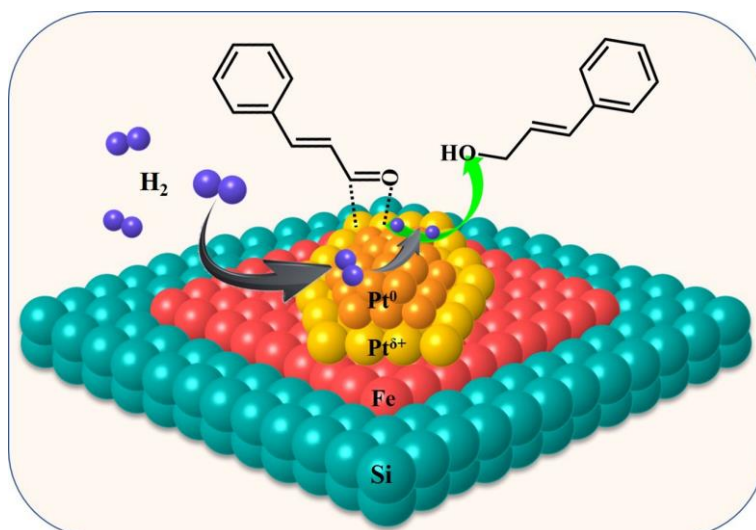


**Figure 11** The hypothesis of CAL adsorption and activation with Pt/FeO<sub>x</sub>/SBA-15 catalyst.

At the Pt-FeO<sub>x</sub> interface, it is proposed that C=O activation takes place through the formation of either a Fe-Pt<sup>2+</sup>...O=C or Fe-Pt<sup>2+</sup>-OH·O=C intermediate. The Pt<sup>2+</sup> sites induce a strong interaction with C=O, resulting in the effective activation of the moiety. Simultaneously, H<sub>2</sub> is dissociative adsorbed onto Pt<sup>0</sup> sites and provide the hydrogen required to reduce the C=O bond. We, therefore, propose that the enhanced activity and selectivity exhibited by the Pt/FeO<sub>x</sub>/SBA-15 catalyst is ascribed to the presence of both Pt<sup>0</sup> and Pt<sup>2+</sup> atoms in the catalyst. For Pt metal particles, the selectivity to COL was determined to be inversely proportional to the Pt particle size. Table S1 suggests that the selectivity to COL does not depend on Pt loadings, but the dispersion of Pt.

#### 4. Conclusions

In conclusion, we developed a highly dispersed Pt catalyst supported on FeO<sub>x</sub>/SBA-15, using a Pt(0)-complex as the precursor. This catalyst was determined to be highly selective to C=O hydrogenation and stable, for the α, β-unsaturated aldehydes hydrogenation. The presence of FeO<sub>x</sub> in the catalyst had two important roles in controlling this chemoselectivity. It assisted with the dispersion of active Pt phase but also assisted directly with the activation of the C=O moiety. Separately, the application of the Pt(0)-complex as the precursor also promoted Pt dispersion, due to the mild reduction conditions required to remove its ligands. This study clearly

demonstrates how the active metal precursors and metal-support interface can dramatically influence catalyst selectivity in hydrogenation reactions. We hope this work will serve as platform for other research, where metal dispersion is advantageous and stability is an issue.

### Conflicts of interest

There are no conflicts to declare.

### Acknowledgments

We acknowledge the financial support from the National Natural Science Foundation (U1910202 and 21978194), the Key Research and Development Program of Shanxi Province (202102090301005) and the Fund for Shanxi “1331 Project”.

### References

- [1] Lan, X.; Wang, T. Highly Selective Catalysts for the Hydrogenation of Unsaturated Aldehydes: A Review. *ACS Catal.*, **2020**, 10, 2764–2790.
- [2] Luo, X.; Jian, Y.; Li, H. Low-Temperature Reduction of Bio-Based Cinnamaldehyde to  $\alpha$ ,  $\beta$ -(Un)Saturated Alcohols Enabled by a Waste-derived Catalyst. *Catal. Commun.*, **2022**, 162, 106391.
- [3] Claus, P. Selective Hydrogenation of  $\alpha$ ,  $\beta$ -Unsaturated Aldehydes and other C=O and C=C Bonds Containing Compounds. *Top. Catal.*, **1998**, 5, 51–62.
- [4] Youngs, T. G. A.; Manyar, H.; Bowron, D. T.; Gladden, L. F.; Hardacre, C. Probing Chemistry and Kinetics of Reactions in Heterogeneous Catalysts. *Chem. Sci.*, **2013**, 4, 3484–3489.
- [5] Bachiller-Baeza, B.; Rodriguez-Ramos, I.; Guerrero-Ruiz, A. Influence of Mg and Ce Addition to Ruthenium Based Catalysts Used in the Selective Hydrogenation of  $\alpha$ ,  $\beta$ -unsaturated Aldehydes. *Appl. Catal., A*, **2001**, 205, 227–237.
- [6] Wang, X.; Liang, X.; Geng, P.; Li, Q. Recent Advances in Selective Hydrogenation of Cinnamaldehyde over Supported Metal-Based Catalysts. *ACS Catal.*, **2020**, 10, 2395–2412.
- [7] Dietrich, C.; Schild, D.; Wang, W.; Kübel, C.; Behrens, S. Bimetallic Pt/Sn-Based Nanoparticles in Ionic Liquids as Nanocatalysts for the Selective Hydrogenation of Cinnamaldehyde. *Z. Anorg. Allg. Chem.*, **2017**, 643, 120–129.
- [8] Liu, Z.; Tan, X.; Li, J.; Lv, C. Easy Synthesis of Bimetal PtFe-Containing Ordered Mesoporous Carbons and their use as Catalysts for Selective Cinnamaldehyde Hydrogenation. *New J. Chem.*, **2013**, 37, 1350–1357.
- [9] Zheng, Q.; Wang, D.; Yuan, F.; Han, Q.; Dong, Y.; Liu, Y.; Niu, X.; Zhu, Y. An Effective Co-promoted Platinum of Co-Pt/SBA-15 Catalyst for Selective Hydrogenation of

- Cinnamaldehyde to Cinnamyl Alcohol. *Catal. Lett.*, **2016**, 146, 1535–1543.
- [10] Dai, Y.; Gao, X.; Chu, X.; Jiang, C.; Yao, Y.; Guo, Z.; Zhou, C.; Wang, C.; Wang, H.; Yang, Y. On the Role of Water in Selective Hydrogenation of Cinnamaldehyde to Cinnamyl Alcohol on PtFe Catalysts. *J. Catal.*, **2018**, 364, 192–203.
- [11] Vu, K. B.; Bukhryakov, K. V.; Anjum, D. H.; Rodionov, V. O. Surface-Bound Ligands Modulate Chemoselectivity and Activity of a Bimetallic Nanoparticle Catalyst. *ACS Catal.*, **2015**, 5, 2529–2533.
- [12] Yuan, K.; Song, T.; Wang, D.; Zhang, X.; Gao, X.; Zou, Y.; Dong, H.; Tang, Z.; Hu, W. Effective and Selective Catalysts for Cinnamaldehyde Hydrogenation: Hydrophobic Hybrids of Metal–Organic Frameworks, Metal Nanoparticles, and Micro- and Mesoporous Polymers. *Angew. Chem., Int. Ed.*, **2018**, 57, 5708–5713.
- [13] Pan, H.; Li, J.; Lu, J.; Wang, G.; Xie, W.; Wu, P.; Li, X. Selective Hydrogenation of Cinnamaldehyde with PtFe<sub>x</sub>/Al<sub>2</sub>O<sub>3</sub>@SBA-15 Catalyst: Enhancement in Activity and Selectivity to Unsaturated Alcohol by Pt-FeO<sub>x</sub> and Pt-Al<sub>2</sub>O<sub>3</sub>@SBA-15 Interaction. *J. Catal.*, **2017**, 354, 24–36.
- [14] Wei, Z.; Zhu, X.; Liu, X.; Xu, H.; Li, X.; Hou, Y.; Liu, Y. Pt-Re/rGO Bimetallic Catalyst for Highly Selective Hydrogenation of Cinnamaldehyde to Cinnamylalcohol. *Chin. J. Chem. Eng.*, **2019**, 27, 369–378.
- [15] Hu, Q.; Wang, S.; Gao, Z.; Li, Y.; Zhang, Q.; Xiang, Q.; Qin, Y. The Precise Decoration of Pt Nanoparticles with Fe Oxide by Atomic Layer Deposition for the Selective Hydrogenation of Cinnamaldehyde. *Appl. Catal., B*, **2017**, 218, 591–599.
- [16] He, S.; Xie, L.; Che, M.; Chan, H. C.; Yang, L.; Shi, Z.; Tang, Y.; Gao, Q. Chemoselective Hydrogenation of  $\alpha$ ,  $\beta$ -Unsaturated Aldehydes on Hydrogenated MoO<sub>x</sub> Nanorods Supported Iridium Nanoparticles. *J. Mol. Catal. A: Chem.*, **2016**, 425, 248–254.
- [17] Bhogeswararao, S.; Srinivas, D. Intramolecular Selective Hydrogenation of Cinnamaldehyde over CeO<sub>2</sub>–ZrO<sub>2</sub>-Supported Pt Catalysts. *J. Catal.*, **2012**, 285, 31–40.
- [18] Tamura, M.; Tokonami, K.; Nakagawa, Y.; Tomishige, K. Effective NbO<sub>x</sub>-Modified Ir/SiO<sub>2</sub> Catalyst for Selective Gas-Phase Hydrogenation of Crotonaldehyde to Crotyl Alcohol. *ACS Sustainable Chem. Eng.*, **2017**, 5, 3685–3697.
- [19] Wei, H.; Liu, X.; Wang, A.; Zhang, L.; Qiao, B.; Yang, X.; Huang, Y.; Miao, S.; Liu, J.; Zhang, T. FeO<sub>x</sub>-Supported Platinum Single-Atom and Pseudo-Single-Atom Catalysts for Chemoselective Hydrogenation of Functionalized Nitroarenes. *Nat. Commun.*, **2014**, 5, 5634.
- [20] Zhao, F.; Ikushima, Y.; Arai, M. Hydrogenation of Nitrobenzene with Supported Platinum Catalysts in Supercritical Carbon Dioxide: Effects of Pressure, Solvent, and Metal Particle Size. *J. Catal.*, **2004**, 224, 479–483.
- [21] Bayram, E.; Lu, J.; Aydin, C.; Browning, N. D.; Özkar, S.; Finney, E.; Gates, B. C.; Finke, R. G. Agglomerative Sintering of an Atomically Dispersed Ir<sub>1</sub>/Zeolite Y Catalyst: Compelling Evidence Against Ostwald Ripening but for Bimolecular and Autocatalytic Agglomeration Catalyst Sintering Steps. *ACS Catal.*, **2015**, 5, 3514–3527.
- [22] Jones, J.; Xiong, H.; DeLaRiva, A. T.; Peterson, E. J.; Pham, H.; Challa, S. R.; Qi, G.; Oh, S.; Wiebenga, M. H.; Hernández, X. I. P. Thermally Stable Single-Atom Platinum-on-Ceria Catalysts via Atom Trapping. *Science*, **2016**, 353, 150–154.
- [23] Qiao, B.; Wang, A.; Yang, X.; Allard, L. F.; Jiang, Z.; Cui, Y.; Liu, J.; Li, J.; Tao, Z. Single-Atom

- Catalysis of CO Oxidation using Pt<sub>1</sub>/FeO<sub>x</sub>. *Nat. Chem.*, **2011**, 3, 634–641.
- [24] Nguyen, L.; Zhang, S.; Wang, L.; Li, Y.; Yoshida, H.; Patlolla, A.; Takeda, S.; Frenkel, A. I.; Tao, F. Reduction of Nitric Oxide with Hydrogen on Catalysts of Singly Dispersed Bimetallic Sites Pt<sub>1</sub>Co<sub>m</sub> and Pd<sub>1</sub>Co<sub>n</sub>. *ACS Catal.*, **2016**, 6, 840–850.
- [25] Ida, S.; Kim, N.; Ertekin, E.; Takenaka, S.; Ishihara, T. Photocatalytic Reaction Centers in Two-Dimensional Titanium Oxide Crystals. *J. Am. Chem. Soc.*, **2015**, 137, 239–244.
- [26] Wang, J.; Zhao, X.; Lei, N.; Li, L.; Zhang, L.; Xu, S.; Miao, S.; Pan, X.; Wang, A.; Zhang, T. Hydrogenolysis of Glycerol to 1,3-propanediol under Low Hydrogen Pressure over WO<sub>x</sub>-Supported Single/Pseudo-Single Atom Pt Catalyst. *ChemSusChem*, **2016**, 9, 784–790.
- [27] Forde, M. M.; Kesavan L.; Saiman, M. I.; He, Q.; Dimitratos, N.; Lopez-Sanchez, J. A.; Jenkins, R. L.; Taylor, S. H.; Kiely, C. J., Hutchings, G. J. High Activity Redox Catalysts Synthesized by Chemical Vapor Impregnation. *ACS Nano*, **2014**, 8, 957–969.
- [28] Kyriakou, G.; Boucher, M. B.; Jewell, A. D.; Lewis, E. A.; Lawton, T. J.; Baber, A. E.; Tierney, H. L.; Flytzani-Stephanopoulos, M.; Sykes, E. C. H. Isolated Metal Atom Geometries as a Strategy for Selective Heterogeneous Hydrogenations. *Science*, **2012**, 335, 1209–1212.
- [29] Lang, R.; Du, X.; Huang, Y.; Jiang, X.; Zhang, T. Single-Atom Catalysts Based on the Metal–Oxide Interaction. *Chem. Rev.*, **2020**, 120, 11986–12043.
- [30] Ketelson, H. A.; Brook, M. A.; Pelton, R.; Heng, Y. M. Hydridosilsesquioxane Modified Silica-Supported Platinum Nanoparticles. *Chem. Mater.*, **1996**, 8, 2195–2199.
- [31] Qin, R.; Liu, K.; Wu, Q.; Zheng, N. Surface Coordination Chemistry of Atomically Dispersed Metal Catalysts. *Chem. Rev.*, **2020**, 120, 11810–11899.
- [32] Maimaiti, Y.; Elliott, S. D. Kinetics and Coverage Dependent Reaction Mechanisms of the Copper Atomic Layer Deposition from Copper Dimethylamino-2-Propoxide and Diethylzinc. *Chem. Mater.*, **2016**, 28, 6282–6295.
- [33] Sun, S.; Zhang, G.; Gauquelin, N.; Chen, N.; Zhou, J.; Yang, S.; Chen, W.; Meng, X.; Geng, D.; Banis, M. N.; Li, R.; Ye, S.; Knights, S.; Botton, G. A.; Sham, T. K.; Sun, X. Single-Atom Catalysis Using Pt/Graphene Achieved Through Atomic Layer Deposition. *Sci. Rep.*, **2013**, 3, 1775.
- [34] Huang, X.; Xia, Y.; Cao, Y.; Zheng, X.; Pan, H.; Zhu, J.; Ma, C.; Wang, H.; Li, J.; You, R.; Wei, S.; Huang, W.; Lu, J. Enhancing both Selectivity and Coking-Resistance of a Single-Atom Pd<sub>1</sub>/C<sub>3</sub>N<sub>4</sub> Catalyst for Acetylene Hydrogenation. *Nano Res.*, **2017**, 10, 1302–1312.
- [35] Gao, G.; Jiao, Y.; Waclawik, E. R.; Du, A. Single Atom (Pd/Pt) Supported on Graphitic Carbon Nitride as an Efficient Photocatalyst for Visible-Light Reduction of Carbon Dioxide. *J Am Chem Soc*, **2016**, 138, 6292–6297.
- [36] Lin, L.; Chen, Z.; Chen, W. Single Atom Catalysts by Atomic Diffusion Strategy. *Nano Res.*, **2021**, 14, 4398–4416.
- [37] Lu, J.; Aydin, C.; Browning, N. D.; Gates, B. C. Imaging Isolated Gold Atom Catalytic Sites in Zeolite NaY. *Angew. Chem., Int. Ed.*, **2012**, 124, 5944–5948.
- [38] Hansen, T. W.; DeLaRiva, A. T.; Challa, S. R.; Datye, A. K. Sintering of Catalytic Nanoparticles: Particle Migration or Ostwald Ripening? *Acc. Chem. Res.*, **2013**, 46, 1720–1730.
- [39] Yan, H.; Cheng, H.; Yi, H.; Lin, Y.; Yao, T.; Wang, C.; Li, J.; Wei, S.; Lu, J. Single-Atom Pd<sub>1</sub>/Graphene Catalyst Achieved by Atomic Layer Deposition: Remarkable Performance in Selective Hydrogenation of 1,3-Butadiene. *J. Am. Chem. Soc.*, **2015**, 137, 10484–10487.
- [40] Iimura, T.; Akasaka, N.; Kosai, T.; Iwamoto, T. A Pt (0) Complex with Cyclic

- (Alkyl)(Amino) Silylene and 1, 3-Divinyl-1, 1, 3, 3-Tetramethyldisiloxane Ligands: Synthesis, Molecular Structure, and Catalytic Hydrosilylation Activity. *Dalton Trans.*, **2017**, 46, 8868–8874.
- [41] Impérator-Clerc, M.; Davidson, P.; Davidson, A. Existence of a Microporous Corona Around the Mesopores of Silica-Based SBA-15 Materials Templated by Triblock Copolymers. *J. Am. Chem. Soc.*, **2000**, 122, 11925–11933.
- [42] Wang, C.; Huang, Z. Controlled Synthesis of  $\alpha$ -Fe<sub>2</sub>O<sub>3</sub> Nanostructures for Efficient Photocatalysis. *Mater. Lett.* **2016**, 164, 194–197.
- [43] He, X.; Deng, Y.; Zhang, Y.; He, Q.; Xiao, D.; Peng, M.; Zhao, Y.; Zhang, H.; Luo, R.; Gan, T. Mechanochemical Kilogram-Scale Synthesis of Noble Metal Single-Atom Catalysts. *Cell Rep. Phys. Sci.*, **2020**, 1, 100004.
- [44] Xue, Y.; Yao, R.; Li, J.; Wang, G.; Wu, P.; Li, X. Efficient Pt–FeO<sub>x</sub>/TiO<sub>2</sub>@SBA-15 Catalysts for Selective Hydrogenation of Cinnamaldehyde to Cinnamyl Alcohol. *Catal. Sci. Technol.*, **2017**, 7, 6112–6123.
- [45] Lewis, L. N.; Colborn, R. E.; Grade, H.; Bryant, G. L.; Sumpter, C. A.; Scott, R. A. Mechanism of Formation of Platinum(0) Complexes Containing Silicon-Vinyl Ligands. *Organometallics*, **1995**, 14, 2202–2213.
- [46] Li, Y.; Zhu, P. F.; Zhou, R. X. Selective Hydrogenation of Cinnamaldehyde to Cinnamyl Alcohol with Carbon Nanotubes Supported Pt-Co Catalysts. *Appl. Surf. Sci.*, **2008**, 254, 2609–2614.
- [47] Sermon, P. A.; Bond, G. C. Hydrogen Spillover. *Catal. Rev.*, **1974**, 8, 211–239.
- [48] Liu, T.; Zeng, X.; Lai, X.; Li, H. Efficient Organic-to-Inorganic Conversion of Polysiloxane by Novel Platinum-Thiol Catalytic System. *Polym. Degrad. Stab.*, **2020**, 176, 109161.
- [49] DeRita, L.; Dai, S.; Lopez-Zepeda, K.; Pham, N.; Graham, G. W.; Pan, X.; Christopher, P. Catalyst Architecture for Stable Single Atom Dispersion Enables Site-Specific Spectroscopic and Reactivity Measurements of CO Adsorbed to Pt Atoms, Oxidized Pt Clusters, and Metallic Pt Clusters on TiO<sub>2</sub>. *J. Am. Chem. Soc.*, **2017**, 139, 14150–14165.
- [50] Ding, K.; Gulec, A.; Johnson, A. M.; Schweitzer, N. M.; Stucky, G. D.; Marks, L. D.; Stair, P. C. Identification of Active Sites in CO Oxidation and Water-Gas Shift over Supported Pt Catalysts. *Science*, **2015**, 350, 189–192.
- [51] Chen, Y.; Ji, S.; Chen, C.; Peng, Q.; Wang, D.; Li, Y. Single-Atom Catalysts: Synthetic Strategies and Electrochemical Applications. *Joule*, **2018**, 2, 1242–1264.
- [52] Tang, H.; Su, Y.; Zhang, B.; Lee, A. F.; Isaacs, M. A.; Wilson, K.; Li, L.; Ren, Y.; Huang, J.; Haruta, M.; Qiao, B.; Liu, X.; Jin, C.; Su, D.; Wang, J.; Zhang, T. Classical Strong Metal–Support Interactions Between Gold Nanoparticles and Titanium Dioxide. *Sci. Adv.*, **2017**, 3, e170023.
- [53] Kim, M. J.; Lee, M. W.; Lee, K. Y. Improved Catalytic Wet Peroxide Oxidation of Phenol over Pt-Fe<sub>2</sub>O<sub>3</sub>/SBA-15: Influence of Platinum Species and DFT Calculations. *Appl. Surf. Sci.*, **2021**, 541, 148409.
- [54] Shi, Y. S.; Yuan, Z. F.; Wei, Q.; Sun, K. Q.; Xu, B. Q. Pt–FeO<sub>x</sub>/SiO<sub>2</sub> Catalysts Prepared by Galvanic Displacement show High Selectivity for Cinnamyl Alcohol Production in the Chemoselective Hydrogenation of Cinnamaldehyde. *Catal. Sci. Technol.*, **2016**, 6, 7033–7037.
- [55] Kuai, L.; Chen, Z.; Liu, S.; Kan, E.; Yu, N.; Ren, Y.; Fang, C.; Li, X.; Li, Y.; Geng, B. Titania Supported Synergistic Palladium Single Atoms and Nanoparticles for Room Temperature

- Ketone and Aldehydes Hydrogenation. *Nat. Commun.*, **2020**, 11, 1–9.
- [56] Pozdnyakova, O.; Teschner, D.; Wootsch, A.; Kröhnert, J.; Steinhauer, B.; Sauer, H.; Toth, L.; Jentoft, F. C.; Knop-Gericke, A.; Paál, Z. Preferential CO Oxidation in Hydrogen (PROX) on Ceria-Supported Catalysts, Part I: Oxidation State and Surface Species on Pt/CeO<sub>2</sub> under Reaction Conditions. *J. Catal.*, **2006**, 237, 1–16.